Synthesis and Characterization of (Fe_3O_4/MWCNTs)/ Epoxy Nanocomposites

Wanda D. Jones, Vijaya K. Rangari, Tarig A. Hassan, Shaik Jeelani

Center for Advanced Materials, Materials Science and Engineering, Tuskegee University, Tuskegee, Alabama 36088

Received 8 August 2008; accepted 15 July 2009
DOI 10.1002/app.31193
Published online 28 January 2010 in Wiley InterScience (www.interscience.wiley.com).

ABSTRACT: A sonochemical technique is used for *in situ* coating of iron oxide (Fe_3O_4) nanoparticles on outer surface of MWCNTs. These Fe_3O_4/MWCNTs were characterized using a high-resolution transmission electron microscope (HRTEM), X-ray diffraction, and thermogravimetric analysis. The as-prepared Fe_3O_4/MWCNTs composite nanoparticles were further used as reinforcing fillers in epoxy-based resin (Epon-828). The nanocomposites of epoxy were prepared by infusion of (0.5 and 1.0 wt %) pristine MWCNTs and Fe_3O_4/MWCNTs composite nanoparticles. For comparison purposes, the neat epoxy resin was also prepared in the same procedure as the nanocomposites, only without nanoparticles. The thermal, mechanical, and morphological tests were carried out for neat and nanocomposites. The compression test results show that the highest improvements in compressive modulus (38%) and strength (8%) were observed for 0.5 wt % loading of Fe_3O_4/MWCNTs. HRTEM results show the uniform dispersion of Fe_3O_4/MWCNTs nanoparticles in epoxy when compared with the dispersion of MWCNTs. These Fe_3O_4/MWCNTs nanoparticles-infused epoxy nanocomposite shows an increase in glass transition (T_g) temperature. © 2010 Wiley Periodicals, Inc. J Appl Polym Sci 116: 2783–2792, 2010

Key words: nanocomposites; coating; thermal properties; mechanical properties; processing

INTRODUCTION

Wide-spread applications of polymer nanocomposite materials have created a new opportunity for the development of high performance, smart, and multifunctional nanocomposites materials. Recently, nanocomposites have shown significant improvements in their mechanical properties. However, the advancement of synthetic methods for developing new types of nanofillers in the last 15 years has sparked an opportunity for the development of multifunctional nanocomposite materials. For example, the nanocomposites with controllable magnetic properties could lead to many advanced applications. Magnetic nanoparticles have shown a variety of unusual magnetic behaviors when compared with the bulk materials, mostly because of surface/interface effects.[1] Magnetic nanocomposites have potential applications in various areas, such as magnetic recording, magnetic data storage devices, toners and inks for xerography, and magnetic resonance imaging.[2,3] Studies in this research area with the focus being aimed on magnetic CNTs are rapidly expanding. The applications of multiwalled carbon nanotubes (MWCNTs) as fillers in different materials have been ever increasing since their discovery.[4] As the CNTs exhibit record high Young's modulus and good elasticity,[5,6] they are expected to find effective use as reinforcements in composite materials. Many studies on CNTs/polymer composites have revealed that good dispersion[7–10] and strong interfacial bonding[10–12] between CNTs and polymer matrix result in strong reinforcement of the polymers. The potential enhancements in the properties of CNTs/polymer nanocomposites have not been fully realized because of several facts. First, CNTs have a nonreactive surface. Second, they lack interfacial bonding with various matrices and can be poorly disperse within those matrices.[13] Third, they have very low solubility in most of the solvents.

Therefore, decoration of CNTs with metal or metal oxides can improve the dispersion of CNTs in solvents[14] or reveal new optical, electric, and magnetic properties of CNTs.[15–18] Many efforts have been devoted to decorate CNTs with diverse organic compound by the covalent attachment, polymer wrapping and surfactant treatment by noncovalent attachment.[19] Various CNT-based composites have been derived from decorating CNTs with metals, metal oxides, and semiconducting nanoparticles.[20–23] The resultant CNTs derivations show promising features for nanoelectric, magnetic, adsorption, optical, and mechanical properties compared with pristine CNTs.[15]

Metal or metal oxide nanoparticles ($\sim$ 10 nm) are easy to deposit on MWCNTs (diameter of $\sim$ 20 nm)

Correspondence to: V. K. Rangari (rangariv@tuskegee.edu).

Contract grant sponsors: National Science Foundation-PREM and RISE Grant.

© 2010 Wiley Periodicals, Inc.

and MWCNTs can be used as carriers.[24,25] To obtain anemometric dimensions in metallic elements, several techniques have been adopted, that is, arc discharge, evaporation, sputtering, and sonochemical method.[25–27] Within the last 10 years, sonochemical processing has served as a useful method to produce metal or metal oxide nanoparticles with novel properties. Sonochemistry arises from the acoustic cavitation phenomenon, that is, the formation, growth, and implosive collapse of bubbles in a liquid medium. Extremely high temperature (>5000 K), pressure (>20 MPa), and very high cooling rates (10^9 K/S)[28] attained during cavitation collapse lead to many unique properties in the irradiated solution. This method has proven to be one of the best methods to fabricate nanomaterials because of its versatility. There are four reasons why. First, this process can be used for the preparation of amorphous products. Second, this method can be used for insertion of nanomaterials into mesoporous materials. Third, the formation of pertinacious micro and nanospheres; and finally, this process allows the deposition of nanoparticles on ceramic and polymeric surfaces.[29] For example, a sonication of volatile precursors in a nonvolatile solvents yields amorphous nanoparticles. This is due to the high cooling rates that prevent the crystallization of the sonication products.[30] While using this method, the reactivity of metal powders can increase by more than 100,000 times. Sonochemistry can drive metal particles together at such high speeds that they melt at the point of collision, and ultrasound can generate microscopic flames in cold liquids.[31–33] In the ultrasonic reaction vessel, sound waves from the transducer radiate through the solution in the tank and cause alternating high and low pressures in the solution. During the low pressure stage, millions of microscopic bubbles form and grow in a process call cavitation. During the high pressure stage, the bubbles collapse or implode, releasing enormous amount of energy. These implosions work in all directions, attacking every surface and all recesses and openings. Many research groups have used ultrasound irradiation techniques in the synthesis of iron oxide (Fe_3O_4)-based nanocomposites.[34,35] Zhang et al. developed a method to synthesize monodispersed Fe_3O_4 nanoparticles in the range of 5–20 nm by ultrasonic method at low temperature and high surfactant concentration.[36] Hiuquen et al. use SDBS modification on the MWCNTs to attach metal ions to the surface by using ammonia solution which facilitates dispersion. By using an ammonia solution, they found it keep positive ion impurities out of the system.[3,37] We have also synthesized the super paramagnetic Fe_3O_4 nanoparticles using sonochemical technique.[38,39] In this study, a similar sonochemical technique is adapted to *in situ* synthesize of Fe_3O_4 nanoparticles in the presence of MWCNTs and a surfactant. These coated Fe_3O_4/MWCNTs were further infused into the epoxy-based resin system using a noncontact defoaming (Thinky) mixer. In this technique, the material container is set at 45° angle inside the mixer and revolves and rotates at high acceleration with the speed of ~ 2000 rpm, dual centrifugal forces were given to the container that keep pressing materials to outward and down along with the slope of inner wall of the container and accomplish powerful mixing and removing air pockets formed in the reaction mixture simultaneously. This technique is noncontact and nonreactive unlike ultrasound and other mixing techniques.[40–42] The thermal and mechanical properties of Fe_3O_4/MWCNTs/epoxy systems will be presented in this article.

EXPERIMENTAL

Materials

The multiwalled carbon nanotubes (10–20 nm in diameter and 0.5–20 μm in length) were purchased from Nanostructured and Amorphous Materials. The two-part epoxy resin Epon-828 was purchased from Miller-Stephenson Chemical, USA. Iron (II) acetate dihydrate and cetyl trimethyl ammonium bromide (CTAB) were purchased from Sigma-Aldrich Chemicals, USA.

Coating and characterization of magnetite nanoparticles on MWCNTs

One gram of iron acetate, 500 mg of cetyl trimethyl ammonium bromide (CTAB, a surfactant), and 1 g of MWCNTs were taken in a 100 mL of double distilled water and irradiated with high-intensity ultrasonic horn (Ti-horn, 20 kHz, 100 W/cm^2) for 3 h at 10°C under argon flow at 50% of amplitude.[38,43] The reaction product was thoroughly washed with double distilled water followed by ethanol. Finally, the products were centrifuged at 10,000 rpm and vacuum dried overnight at room temperature.

Characterization

X-ray diffraction. X-ray diffraction (XRD) analysis was carried out to study the effect of Fe_3O_4 coating on MWCNTs using a Rigaku D/MAX 2200 X-ray Diffractometer. The XRD samples were prepared by uniformly spreading Fe_3O_4 or Fe_3O_4/MWCNTs powder on a quartz sample holder. These XRD tests were conducted at room temperature from 10° to 80° of two thetas.

Transmission electron microscopy. A high-resolution transmission electron microscopy (HRTEM) has been performed on Fe_3O_4/MWCNTs nanoparticles, 0.5 wt

% of MWCNTs/Epon-828, and 0.5 wt % of Fe_3O_4/MWCNTs/Epon-828 using a JOEL-2010. Energy dispersive spectroscopy (EDS) was also carried out using oxford EDS-spectrometer on JEOL 2010 TEM. The samples for HRTEM were prepared by dispersion of Fe_3O_4/MWCNTs nanoparticles in ethanol and placed a drop of solution on a copper grid (copper grid-200 mesh) and dried in air, then used for HRTEM/EDS analysis. The 0.5 wt % of MWCNTs/Epon-828 and 0.5 wt % of Fe_3O_4/MWCNTs/Epon-828 nanocomposite samples were prepared using a Leica EM UC6 microtome and tested for HRTEM/EDS analysis.

Thermal analysis. Thermogravimetric analysis (TGA) of MWCNTs and Fe_3O_4-coated MWCNTs were carried out under nitrogen and oxygen gas atmospheres on a Mettler Toledo TGA/SDTA 851^e apparatus from 30 to 800°C at a heating rate of 10°C/min. The weight of samples used for TGA tests was ~ 10–20 mg.

Preparation and characterization of MWCNTs/epoxy nanocomposites

Preparation

Before curing, the epoxy resin was mixed with known weight percentages of MWCNTs (0.5 and 1 wt %) using a Thinky hybrid defoaming mixer ARE-250 for 10 min. A stoichiometric amount (26 wt %) of the curing agent (epicure W) was added to the reaction mixture containing epoxy and MWCNTs or Fe_3O_4/MWCNTs and mixed for another 10 min. The mixture was degassed using a vacuum oven for 30 min, and the final reaction mixture was transferred into a stainless steel mold for curing. The epoxy resin with and without MWCNTs or Fe_3O_4 nanoparticles were cured at 120°C for 2 h and postcured for 2 h at 150°C in an oven.

Thermal analysis (DSC)

Differential scanning calorimetry (DSC) experiments were carried out using a Mettler Toledo DSC 822^e from 30 to 300°C at a heating rate of 10°C/min under nitrogen atmosphere.

Dynamic mechanical analysis

The DMA studies of neat Epon-828 and the nanocomposite samples were carried out using a TA Instruments DMA 2980 in the single cantilever mode. The strain amplitude of 10 μm and an oscillatory frequency of 1 Hz were used. The samples were ramped from room temperature to 200°C using a ramp rate of 3°C/min in air. The storage modulus was measured. The width of the samples was 12 mm, and the span length to thickness ratio was 10. The test was carried out according to ASTM D 4065-01.

Scanning electron microscopy

SEM studies were carried out to study the microstructure of neat Epon-828, 0.5 wt % of uncoated MWCNTs, and 0. 5 wt % of Fe_3O_4-coated MWCNTs. The SEM samples were prepared using a precisely cut sample and placing on a sample holder using a silver paint. The samples were coated with gold palladium to prevent the charge buildup by electrons. Sputtering was done using Hummer 6.2 to coat the samples. Resulting samples were analyzed using a JEOL JSM 5800.

Mechanical characterization

Mechanical tests were carried out to determine the compressive and flexural properties of neat Epon-828 and nanocomposite systems. The compression specimens were prepared according to an ASTM standard C365-57 (size 12.7 mm width and 25.4 mm in length). The specimens were tested using a servo-hydraulically controlled Material Testing System MTS-810 with the capacity of 100 kN. The tests were carried out in displacement control mode at a crosshead speed of 1.27 mm/min. To maintain evenly distributed compressive loading, each specimen was sanded and polished so that the opposite faces were parallel to each other. The load and crosshead displacement data were recorded using Test Ware-SX software, which also controlled the test conditions. The load-deflection data recorded by the data acquisition system were then converted to stress–strain

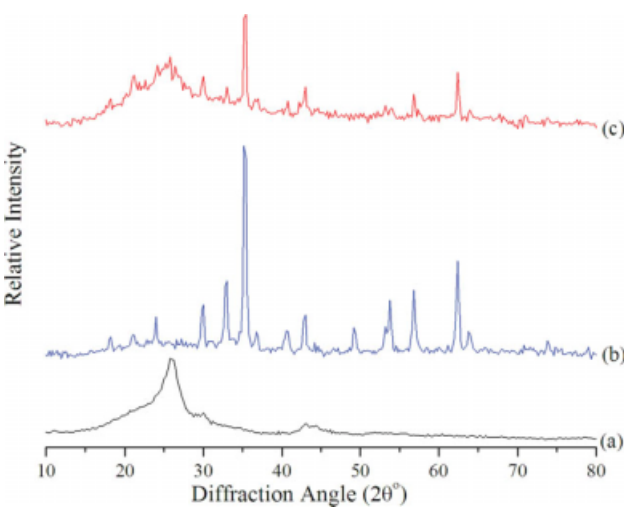

Figure 1 X-ray diffraction patterns of (a) as-received MWCNTs, (b) as-prepared Fe_3O_4 nanoparticles, and (c) as-prepared Fe_3O_4/MWCNTs nanoparticles. [Color figure can be viewed in the online issue, which is available at www.interscience.wiley.com.]

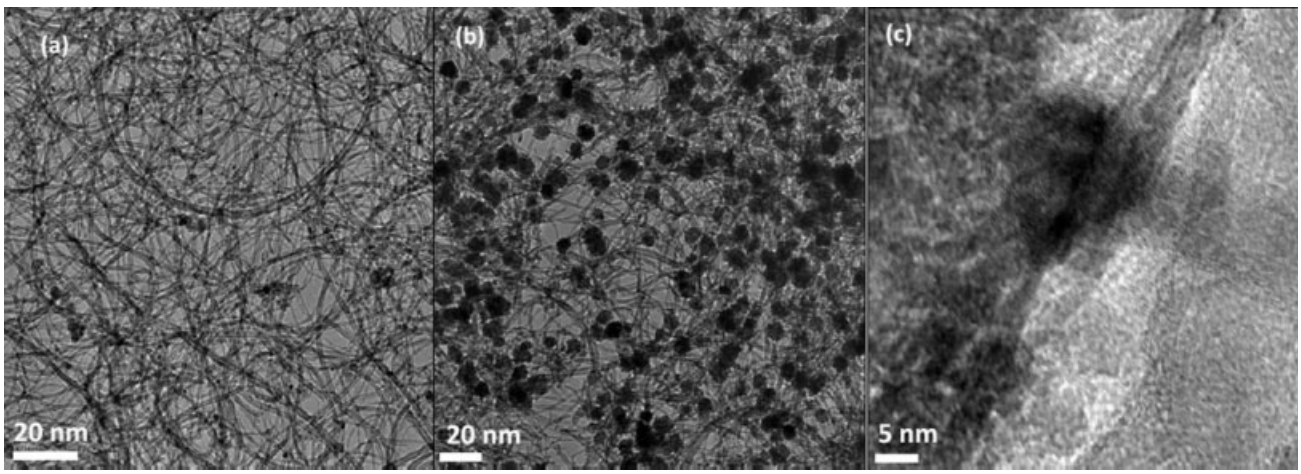

Figure 2 TEM micrographs of (a) pristine MWCNTs, (b) Fe_3O_4 nanoparticles coated on MWCNTs, and (c) high-resolution TEM of Fe_3O_4 coated on MWCNTs.

curves. Flexural specimens were prepared according to ASTM standard D 790-01. The specimens were tested using Zwick/Roell Material Testing Machine. The load cell used on the Zwick/Roell machine is ~ 2.5 kN. The test was carried out in displacement control mode and the crosshead speed was 2 mm/min. TestXpert software was used to analyze the load-deflection data recorded by the data acquisition system.

RESULTS AND DISCUSSION

XRD analysis

Figure 1(a) shows the XRD pattern of the pristine MWCNTs. It can be seen that the diffraction peaks at $2\Theta = 26^\circ$ and 43° are assigned to (002) and (110) planes of MWCNTs, respectively. The XRD pattern of as-prepared Fe_3O_4 nanoparticles is shown in Figure 1(b). All the diffraction peaks of Figure 1(b) are assigned to the Fe_3O_4 nanoparticles, and they match very well (JCPDS card No. 19-0629) of magnetite. Figure 1(c) represents the XRD pattern of the 0.5 wt % of Fe_3O_4/MWCNTs. The characteristic peaks of MWCNTs and Fe_3O_4 still exist with low intensity peaks at the same 2Θ angles. No peak shift was observed. It should be noted that the peak intensities of MWCNTs decrease after coating with Fe_3O_4 nanoparticles on MWCNTs. These results indicate that the Fe_3O_4 nanoparticles are coated on MWCNTs. Similar results were also observed by other researchers.[3]

TEM studies

TEM Studies have been carried out to understand the extent of Fe_3O_4 coating on MWCNTs. Figure 2(a) shows the TEM picture of the pristine MWCNTs. The particles sizes measure from the figures are ~ 10–20 nm in diameter and 0.5–2 μm in length. The pristine MWCNTs are entangled with minimal agglomeration. Figure 2(b) represents the TEM micrograph of Fe_3O_4 nanoparticles coated on MWCNTs. The micrograph clearly shows that the Fe_3O_4 nanoparticles are uniformly coated all over the MWCNTs. To estimate the Fe_3O_4 nanoparticle sizes, a high-magnification micrograph was taken and presented in Figure 2(c). This micrograph clearly shows that the particle sizes are ~ 2–5 nm in diameter, spherical in shape, and particles are well attached on the surface of MWCNTs.

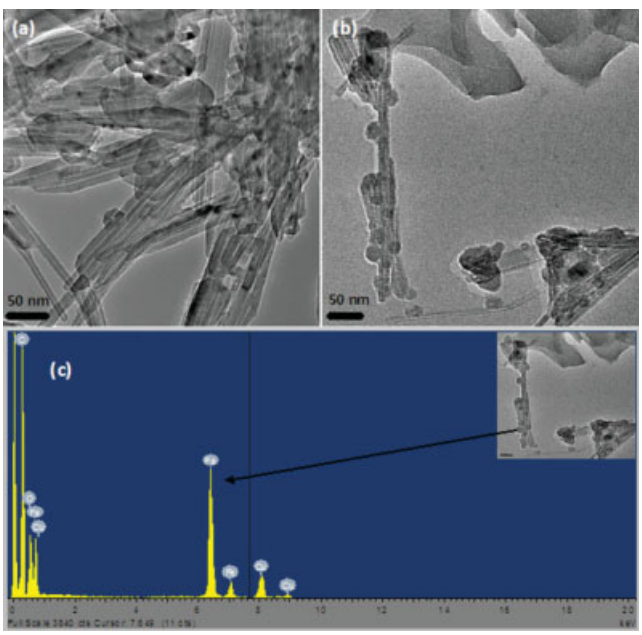

Figure 3 TEM micrographs of (a) pristine MWCNTs dispersion in Epon-828, (b) Fe_3O_4 nanoparticles coated on MWCNTs dispersion in Epon-828, and (c) EDS micrograph showing Fe_3O_4 nanoparticle on MWCNTs in Epon-828 epoxy. [Color figure can be viewed in the online issue, which is available at www.interscience.wiley.com.]

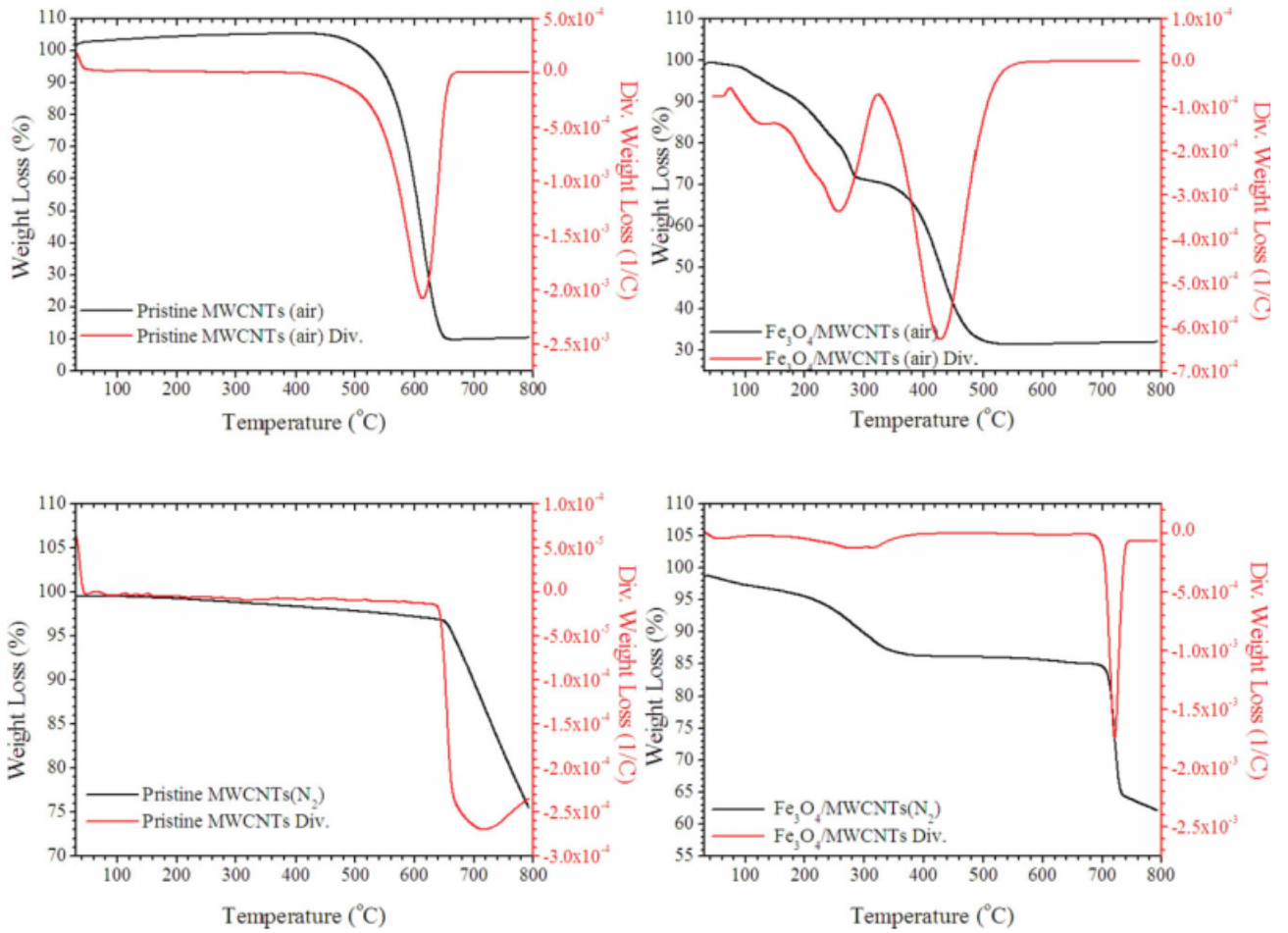

Figure 4 Thermogravimetric analysis (TGA) of pristine MWCNTs and Fe_3O_4-coated MWCNTs in air and nitrogen atmospheres. [Color figure can be viewed in the online issue, which is available at www.interscience.wiley.com.]

TEM studies were also carried out to study the dispersion of MWCNTs and Fe_3O_4/MWCNTs in the Epon-828 resin. The TEM micrographs of nanocomposite samples of 0.5 wt % MWCNTs/Epon-828 and 0.5 wt % Fe_3O_4/MWCNTs/Epon-828 are presented in Figure 3(a,b), respectively. Figure 3(a) shows that the MWCNTs are well dispersed in the Epon-828 resin. As seen in micrograph [Fig. 3(a)], the MWCNTs are completely covered with resin and particles. They are well dispersed in the Epon-828 resin when compared with the pristine MWCNTs [Fig. 2(a)]. The dispersion of Fe_3O_4-coated MWCNTs in Epon-828 resin is shown in Figure 3(b). This figure clearly shows that the Fe_3O_4-coated MWCNTs are well dispersed over the entire volume of the Epon-828 resin with no agglomeration. In this micrograph, we can also see that the Fe_3O_4 nanoparticles adhere on the MWCNTs after dispersion in the Epon-828 resin. This clearly shows that the noncontact mixing method is efficient in mixing the coated nanoparticles in Epon-828 resin. To confirm the coating of Fe_3O_4 nanoparticles on MWCNTs, the EDS analysis was carried out and the results are presented in Figure 3(c). These results show the presence of Fe, O, and C elements at nanoscale. The Cu peaks are assigned to the copper grid.

TGA analysis

The TGA graphs are shown in Figure 4 and the results are summarized in Table I. They illustrate the decomposition behavior of the pristine and Fe_3O_4-coated MWCNTs in air and nitrogen atmospheres. When these samples are heated in air up to 800°C from 30°C, the pristine and Fe_3O_4-coated MWCNTs decompose differently. The pristine

TABLE I
TGA Analysis of Pristine and Magnetite-Coated MWCNTs in Oxygen (O_2) and Nitrogen (N_2) Atmospheres

Sample	(%) Residue at 800°C	Major decomposition Temperature
Pristine MWCNTs-N_2	77	710
Pristine MWCNTs-O_2	10	610
MWCNTs-Fe_3O_4-N_2	62	724
MWCNTs-Fe_3O_4-O_2	32	430

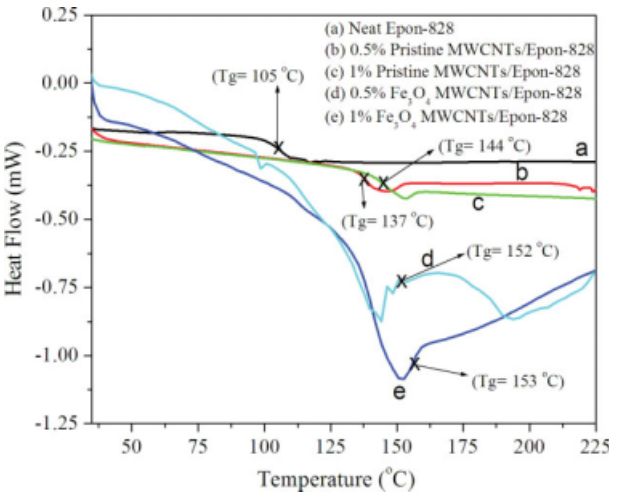

Figure 5 DSC curves of neat Epon-828 and nanocomposite systems. [Color figure can be viewed in the online issue, which is available at www.interscience.wiley.com.]

MWCNTs decompose at ~ 610°C, where as the Fe_3O_4-coated MWCNTs decompose at ~ 430°C. The Fe_3O_4-coated MWCNTs decomposed ~ 180°C earlier than the pristine MWCNTs in the presence of nitrogen. The possible reason for the early decomposition of MWCNTs in the presence of the Fe_3O_4 nanoparticles is that the Fe_3O_4 nanoparticles may act as a catalyst to foster a faster decomposition rate. On the other hand, when these samples were heated in a nitrogen atmosphere, the major decomposition was at 710°C for pristine MWCNTs and 724°C for Fe_3O_4-coated MWCNTs. The Fe_3O_4-coated MWCNTs decomposed ~ 14°C later than the pristine MWCNTs. These results clearly show that the decomposition behavior of pristine MWCNTs and Fe_3O_4-coated MWCNTs are quite different in the presence of air and nitrogen atmospheres. The catalytical decomposition of MWCNTs in the presence of air and Fe_3O_4 is at lower temperature than in the nitrogen and Fe_3O_4 nanoparticles. To estimate the percentage coating of Fe_3O_4 nanoparticles on MWCNTs, the mass of the residue at 800°C was estimated from the TGA data in the presence of air and nitrogen. These residues masses by weight percentage are presented in Table I. The difference in the residue of MWCNTs (10 wt %) and Fe_3O_4-coated MWCNTs (32 wt %) in the presence of air is about 20 wt %. These results are within the limits of experimental errors calculated from the yield of Fe_3O_4 nanoparticles synthesized without MWCNTs.

TABLE II
DSC Analysis of Neat Epon-828 and Nanocomposite Systems

Sample	Glass transition T_g
Neat Epon-828	105
0.5% Pristine MWCNTs/Epon-828	144
1% Pristine MWCNTs/Epon-828	137
0.5% Fe_3O_4 MWCNTs/Epon-828	152
1% Fe_3O_4 MWCNTs/Epon-828	153

TABLE III
DMA Results of Neat Epon-828 and Nanocomposite Systems

Sample	Storage modulus (MPa)	Percent (%) increase
Neat Epon-828	1603 ± 156	–
0.5% Pristine MWCNTs/Epon-828	2059 ± 131	+28
1% Pristine MWCNTs/Epon-828	2304 ± 179	+44
0.5% Fe_3O_4 MWCNTs/Epon-828	2065 ± 74	+29
1% Fe_3O_4 MWCNTs/Epon-828	2161 ± 263	+38

DSC analysis

DSC analyses were carried out to study the effect of magnetite nanoparticles-coated MWCNTs infusion in Epon-828 nanocomposite materials by measuring the T_g. Figure 5 depicts the DSC curves of all five systems and the results are summarized in Table II. All the samples were cured at 120°C for 2 h and postcuring at 150°C for another 2 h. The T_gs determined as the inflection points of the heat flow curves.[39,44] These results suggest that the T_g has increased by 39°C from neat epoxy to 0.5 wt % MWCNTs system. This increase in T_g is due to the presence of MWCNTs, usually T_g increases with increasing crosslinking density of epoxy resins because of the restriction in molecular chain mobility imposed by crosslinking.[45,46] This effect can be understood in terms of decreasing free volume.[47] In the contrary, in Figure 5(c), the T_g of

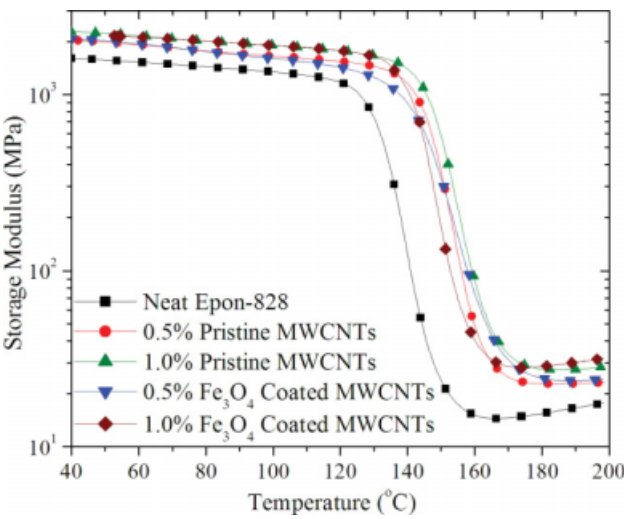

Figure 6 DMA of the neat Epon-828 and nanocomposite systems. [Color figure can be viewed in the online issue, which is available at www.interscience.wiley.com.]

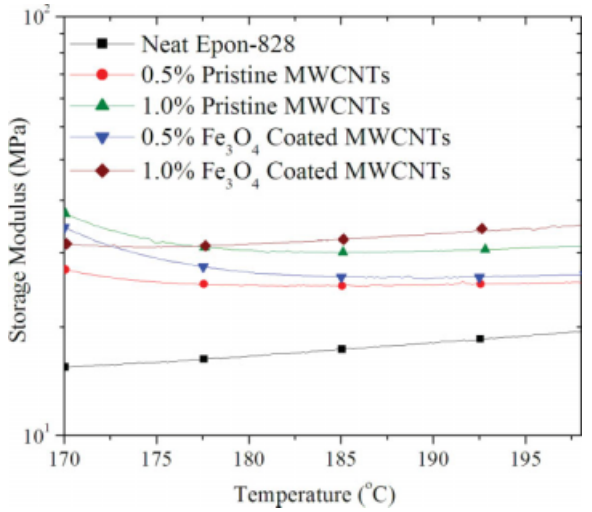

Figure 7 DMA rubbery plateau region of neat Epon-828 and nanocomposite systems. [Color figure can be viewed in the online issue, which is available at www.interscience.wiley.com.]

1 wt % MWCNTs system has decreased when compared with the 0.5 wt % of MWCNTs/Epon-828 composite. The reason for this decrease in T_g could be the start of agglomeration of MWCNTs in Epon-828 epoxy resin. With relatively higher loading (1 wt % of MWCNTs), the number of particles are surely high because of their nanosize and extremely low density, and it becomes more and more difficult to disperse uniformly. Once the particles start to agglomerate, the interaction is more between the particles rather than the particle and the polymer. We believe at that stage, the particles begin to act as impurities in the bulk polymer. Also, we believe that the volume of the agglomerated particle is much larger and it can no longer occupy the free space. The agglomerated particles cannot, therefore, impose any restrictions on molecular mobility. On the other hand, the lumped particles can reduce the crosslinking density of the polymer and lower the T_g if we further increase the loading of MWCNTs. Where as the Figure 5(d), the T_g of Fe_3O_4-coated MWCNTs/Epon-828 system has further increased (9°C) when compared with the 0.5 wt % MWCNTs-infused Epon-828. The reason for this increase in T_g could be the increase in dispersion of MWCNTs resulted in an increase in the crosslinking

TABLE IV
DMA Results of the Storage Modulus in Rubbery Plateau Region

Sample	Storage modulus (MPa)
Neat Epon-828	14.9
0.5% Pristine MWCNTs/Epon-828	23.0
1% Pristine MWCNTs/Epon-828	29.7
0.5% Fe_3O_4 MWCNTs/Epon-828	26.9
1% Fe_3O_4 MWCNTs/Epon-828	28.4

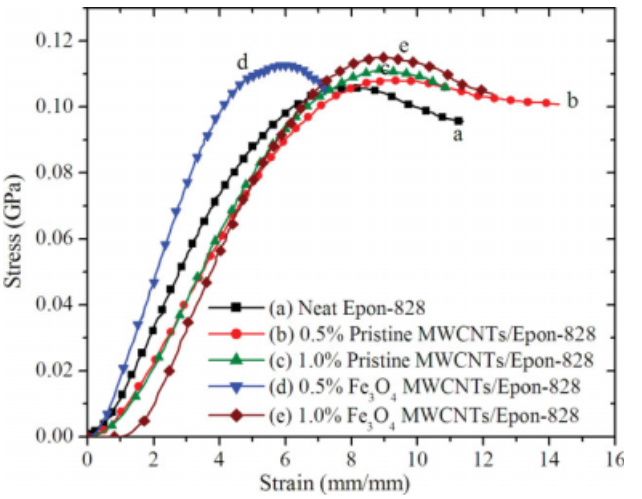

Figure 8 Compression stress–stain curves of (a) neat Epon-828, (b) 0.5 wt % of pristine MWCNTs/Epon-828, (c) 1 wt % of pristine MWCNTs/Epon-828, (d) 0.5 wt % of Fe_3O_4-coated MWCNTs/Epon-828, and (e) 1 wt % Fe_3O_4-coated MWCNTs/Epon-828. [Color figure can be viewed in the online issue, which is available at www.interscience.wiley.com.]

of Epon-828 in the presence of Fe_3O_4 nanoparticles. These results clearly suggest that coating of magnetite nanoparticles on MWCNTs increases their dispersion in Epon-828 resin. These results are consistence with our earlier results,[48,49] and also the DMA results indicate the increase in crossliking for magnetite-coated MWCNTs in Epon-828.

Dynamic mechanical analysis results

DMA studies were conducted to measure the storage modulus[50] and the results are presented in Table III and shown in Figure 6. These results clearly indicate that the addition of 1 wt % of MWCNTs

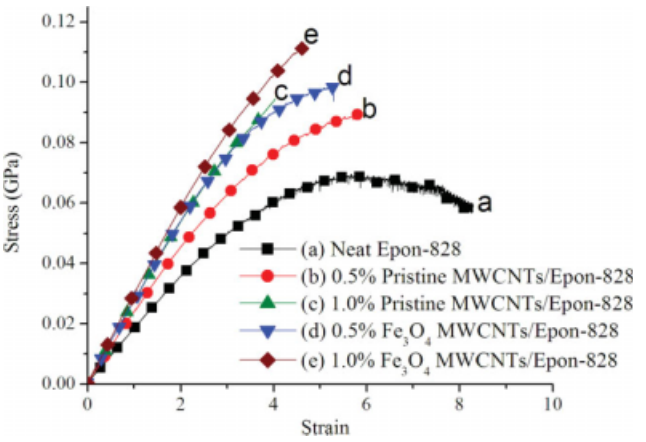

Figure 9 Flexural stress–stain curves of (a) neat Epon-828, (b) 0.5 wt % of pristine MWCNTs, (c) 1 wt % of pristine MWCNTs, (d) 0.5 wt % of Fe_3O_4-coated MWCNTs/Epon-828, and (e) 1 wt % Fe_3O_4-coated MWCNTs/Epon-828. [Color figure can be viewed in the online issue, which is available at www.interscience.wiley.com.]

TABLE V
Quasi-Static Compression Properties of Neat Epon-828 and Nanocomposite Systems

Sample	Ultimate stress (GPa)	Compressive modulus (GPa)
Neat Epon-828	0.106	1.67
0.5% Pristine MWCNTs/Epon-828	0.107	2.121
1% Pristine MWCNTs/Epon-828	0.105	2.026
0.5% Fe_3O_4 MWCNTs/Epon-828	0.112	2.436
1% Fe_3O_4 MWCNTs/Epon-828	0.115	2.306

and 1 wt % of Fe_3O_4-coated MWCNTs has significant effect on the storage modulus. The addition of 1 wt % of MWCNTs and 1 wt % of Fe_3O_4-coated MWCNTs in Epon-828 increases $\sim$ 44 and 38% in storage modulus when compared with the neat Epon-828, respectively. Improvement occurs in the dispensability by increasing the surface polarity inducing the corporation of MWCNTs into the matrix resulting in a larger improvement in the ultimate strength. The rubbery plateau region of DMA test results is shown in Figure 7 and presented in Table IV. These results can be used to estimate the number of entanglements or crosslinks. The modulus in the plateau region is proportional to either the number of crosslinks or the chain length between entanglements. This is often expressed in shear as

$$G' \approx (\rho RT)/M_e$$

where G' is the modulus of the plateau region at a specific temperature, ρ is the polymer density, and M_e is the molecular weight between entanglements. In practice, the relative modulus of the plateau region tells us about the relative changes in $M\sim$ or the number of crosslinks compared to a standard material. The rubbery plateau is also related to the degree of crystallinity in a material, although DSC is a better method for characterizing crystallinity than DMA.[50] In this region, we see an increase in the modulus for 1 wt % of MWCNTs and Fe_3O_4-coated MWCNTs in Epon-828 epoxy, which is a strong indication that there is an increase in the crosslinking as well.

Mechanical analysis

To study the effect of coating of MWCNTs on mechanical properties, flexural and quasi-static compressive properties of the Fe_3O_4/MWCNTs–Epon-828 epoxy were measured. The stress–strain curves of the neat Epon-828 and coated MWCNTs and uncoated MWCNTs-infused Epon-828 resin are shown in Figures 8 and 9. The stress and modulus data are presented in Table V. The test results shown in Table V clearly indicate that the compressive strength and modulus properties of the nanocomposite increase with the coated MWCNTs-reinforced epoxy matrix when compared with the unreinforced neat resin composite. The strength and modulus increased by 8 and 38%, respectively, when compared with the neat sample values.

Figure 8 shows that the compressive modulus increases maximum for the 0.5% loading of magnetite-coated MWCNTs. However, the compressive strength increased maximum for the 1% loading of magnetite MWCNTs and shown lower strain to failure when compared with the unreinforced neat epoxy. The increase in strain to failure was observed for 0.5% uncoated MWCNTs-reinforced nanocomposite.

A flexure test produces a tensile stress in the convex side of the specimen and compression stress in the concave side. This creates an area of shear stress along the midline. Flexure test measures the force required to bend a specimen under three-point loading condition. In a three-point test, the area of uniform stress is quite small and point concentrated under the center loading point The flexural test measures were carried out under a three-point bend loading conditions at ambient temperature. Figure 9 shows flexural stress–stain curves of (a) neat Epon-828, (b) 0.5 wt % of uncoated MWCNTs, (c) 1 wt % of uncoated MWCNTs, (d) 0.5 wt % of magnetite-coated MWCNTs, and (e) 1 wt % magnetite-coated MWCNTs. The rest of the results are presented in Table VI. These results show that there is a gradual increase in the flexural modulus and strength. With the addition of the pristine MWCNTs (1 wt %) and coated MWCNTs (1 wt %), the strength increases to 20 and 50%, respectively, when compared with the neat Epon-828 epoxy.

TABLE VI
Flexural Properties of Neat Epon-828 and Nanocomposite Systems

Sample	Ultimate flexural strength (GPa)	Flexural modulus (GPa)
Neat Epon-828	0.078	2.19
0.5% Pristine MWCNTs/Epon-828	0.093	2.34
1% Pristine MWCNTs/Epon-828	0.094	2.67
0.5% Fe_3O_4 MWCNTs/Epon-828	0.099	2.70
1% Fe_3O_4 MWCNTs/Epon-828	0.117	2.84

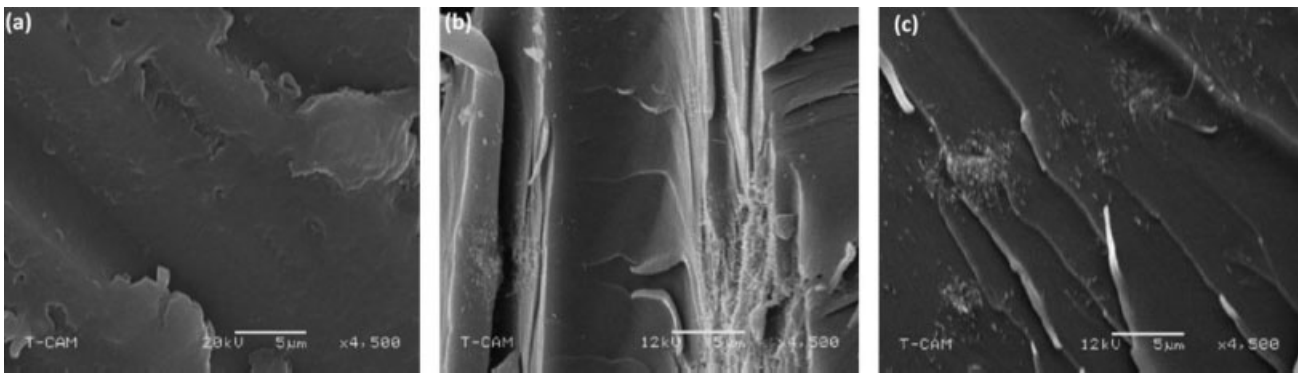

Figure 10 SEM micrographs of (a) neat Epon-828, (b) 1.0 wt % of pristine MWCNTs/Epon-828, (c) 1.0 wt % of Fe_3O_4-coated MWCNTs/Epon-828 epoxy.

SEM analysis

SEM analysis was carried out to investigate the fracture surfaces of neat epoxy, Fe_3O_4-coated MWCNTs, and uncoated MWCNTs in the Epon-828 nanocomposites and shown in Figure 10. The fracture surfaces shown in Figure 10 represent the cross-sectional view of (a) neat Epon-828, (b) 1.0 wt % of uncoated MWCNTs in Epon-828, and (c) 1.0 wt % of magnetite-coated MWCNTs in Epon-828 epoxy. As seen in the Figure 10, samples failed as a combination of breaking of small fragments and propagation of cracks originating from materials flaws in the as-prepared samples. It is observed in the Figure 10 that the polymer matrix cracks are more of a ductile nature in the neat Epon-828 epoxy as opposed to a brittle failure in case of Fe_3O_4-coated and uncoated MWCNTs-infused Epon-828 epoxy resin. These results are consistence with our previous results on SiC nanoparticles in SC-15 epoxy resin,[48] and by introducing nanoparticles the epoxy polymer matrix becomes more brittle. Figure 10(b,c) shows that the cracks spread out in radial manner in both Fe_3O_4-coated and uncoated MWCNTs-infused Epon-828, but coalesced more predominantly only in the Fe_3O_4-coated MWCNTs-infused Epon-828, which indicate again the brittle nature of failure modes. These results clearly show that the infusion of coated and uncoated MWCNTs in to Epon-828 shifted from a relatively ductile to a brittle materials.

CONCLUSIONS

A sonochemical technique has been developed for *in situ* coating of magnetite nanoparticles on MWCNTs. TGA results show that the coated MWCNTs maintain thermal stability at high temperatures. DMA results show increase in storage moduli for nanocomposites with addition of MWCNTs. DSC results show that there is an increase in T_g for Fe_3O_4-coated MWCNTs nanocomposites. Compressive stress–strain results also indicate that there is a significant increase in strength and modulus about 8 and 38%, respectively. Flexural stress–strain results also indicate 50% increase in strength and 30% increase in modulus. TEM shows improvement in dispersion of MWCNTs in epoxy system with magnetite coating. This coating technique of MWCNTs can be applied to other nanoparticles to enhance the thermal and mechanical properties of nanocomposite materials and can be used for various applications.

References

1. Armelao, L.; Barreca, D.; Bottaro, G.; Gasparotto, A.; Gross, S.; Maragno, C.; Tondello, E. Coord Chem Rev 2006, 250, 1294.
2. Atkins, P.; Overton, T.; Rourke, J.; Weller, M.; Armstrong, F. Shriver & Atkins Inorganic Chemistry, 4th ed.; Oxford University Press: New York, 2006; p 643.
3. Huiquin, C.; Meifang, Z.; Yaogang, L. J. Solid State Chem 2006, 179, 1208.
4. Iijima, S. Nature 1991, 354, 56.
5. Wong, E. W.; Sheehan, P. E.; Lieber, C. M. Science 1997, 277, 1971.
6. Wang, C.; Guo, Z.; Fu, S.; Wu, W.; Zhu, D. Prog Polym Sci 2004, 29, 1079.
7. Mohammad, M.; Karen, I. W. Macromolecules 2006, 39, 5194.
8. Dalton, A. B.; Collins, S.; Munoz, E.; Razal, J. M.; Ebron, V. H.; Ferraris, J. P.; Coleman, J. N.; Kim, B. G.; Baughman, R. H. Nature 2003, 423, 703.
9. Gong, X. Y.; Liu, J.; Baskaran, S.; Voise, R. D.; Young, J. S. Chem Mater 2006, 12, 1049.
10. Jin, Z. X.; Pramoda, K. P.; Goh, S. H.; Xu, G. Q. Mater Res Bull 2002, 37, 271.
11. Qian, D.; Dickey, E. C.; Andrews, R.; Rantell, T. Appl Phys Lett 2000, 76, 2868.
12. Xu, X. J.; Thwe, M. M.; Shearwood, C.; Liao, K. Appl Phys Lett 2002, 81, 2833.
13. Cadek, M.; Coleman, J. N.; Barron, V.; Hedicke, K.; Blau, W. J. Appl Phys Lett 2002, 81, 5123.
14. Oh-Kil, K.; Jongtae, J.; Jeffrey, W. B.; Steven, K.; Pehr, P. E.; Leonard, J. B. J Am Chem Soc 2003, 125, 4426.
15. Chin, K. C.; Gohel, A.; Ielim, H.; Ji, W.; Chong, G. L.; Lim, K. Y.; Sow, C. H.; Wee, A. T. S. Chem Phys Lett 2004, 383, 72.
16. Oymak, H.; Erkoc, S. Chem Phys 2004, 300, 277.
17. Watts, P. C. P.; Hsu, W. K.; Randall, D. P.; Kotzeva, V.; Chen, G. Z. Chem Mater 2002, 14, 4505.
18. Wu, Y. H.; Qiao, P. W.; Qiu, J. J.; Chong, T. C.; Low, T. S. Nano Lett 2002, 2, 161.

19. He, B. J.; Sun, W. L.; Wang, M.; Shen, Z. Q. Mater Chem Phys 2005, 95, 202.
20. Vasilios, G.; Vasilios, T.; Dimitrios, G.; Dimitrios, P. Chem Mater 2005, 17, 1613.
21. Tsang, C.; Chen, Y. K.; Harris, P. J. F.; Green, M. L. H. Nature 1994, 372, 159.
22. Pradhan, B. K.; Toba, T.; Kyotani, T.; Tomita, A. Chem Mater 1998, 10, 2510.
23. Monthioux, M. Carbon 2002, 40, 1809.
24. Wei, J.; Ding, J.; Zhang, X.; Wu, D.; Wang, Z.; Lao, J.; Wang, K. Mater Lett 2005, 59, 322.
25. Gozzi, D.; Latini, A.; Capannelli, G.; Canepa, F.; Napolento, M.; Cim, M. R.; Tropeano, M. J. Alloys Comp 2006, 419, 32.
26. Chazelas, C.; Colbert, J. F.; Jarridge, J.; Fauchais, P. J Eur Ceram Soc 2007, 27, 947.
27. Ceylan, A.; Ozcan, S.; Ni, C.; Shah, S. I. J Magn/Magn Mater 2008, 320, 857.
28. Suslick, K. Sci Am 1989, 260, 80.
29. Suslick, K. Modem Synthetic Methods; Springer-Verlag: New York, 1986; Vol. 4, p 1.
30. Boudjouk, P. J Chem Ed 1986, 63, 427.
31. Suslick, K.; Flint, E. B. Nature 1987, 330, 553.
32. Suslick, K. Ultrasound: Its Chemical, Physical and Biological Effects; VCH Publishers: New York, 1988.
33. Gedanken, A. Ultrason Sonochem 2004, 11, 47.
34. Sun, J.; Gao, L. J Electrogram 2006, 17, 91.
35. Loera, A. G.; Cara, F.; Dumon, M.; Pascault, J. P. Macromolecules 2002, 35, 6291.
36. Zhang, G. Q.; Wu, H. P.; Ge, M. Y.; Jiang, Q. K.; Chen, L. Y.; Yao, J. M. Mater Lett 2007, 61, 2204.
37. Hiuquen, C.; Meifang, Z.; Yaogang, L. J Magn/Magn Mater 2006, 305, 321.
38. Rangari, V. K.; Koltypin, Y.; Felner, I.; Gedanken, A. Mater Sci Eng A 2000, 286, 101.
39. Rangari, V. K.; Koltypin, Y.; Cohen, Y. S.; Aurbach, D.; Palchik, O.; Felner, I.; Gedanken, A. J Mater Chem 2000, 10, 1125.
40. Isobe, T.; Kameshima, Y.; Nakajima, A.; Okada, K. J Eur Ceram Soc 2007, 27, 61.
41. Allaoui, A.; Hoa, S. V.; Pugh, M. D. Comput Sci Technol 2008, 68, 410.
42. Rao, P.; Iwasa, M.; Tanaka, T.; Kondoh, I. Ceram Int 2003, 29, 209.
43. Rangari, V. K.; Koltypin, Y.; Xu, X. N.; Yeshurun, Y.; Felner, I.; Gedanken, A. J Appl Phys 2001, 89, 6324.
44. Loera, A. G.; Cara, F.; Dumon, M.; Pascault, J. P. Macromolecules 2002, 3, 56291.
45. Cook, W. D.; Mehrabi, M.; Edward, G. H. Polymer 1999, 40, 1209.
46. Monstserrat, S. J Polym Sci Part B: Polym Phys 1994, 32, 509.
47. Monstserrat, S. Polymer 1995, 36, 435.
48. Rodgers, R. M.; Mahfuz, H.; Rangari, V. K.; Chisholm, N.; Jeelani, S. Macromol Mater Eng 2005, 290, 423.
49. Rangari, V. K.; Hassan, T. A.; Zhou, Y.; Mahfuz, H.; Jeelani, S.; Prorok, B. C. J Appl Polym Sci 2007, 103, 308.
50. Menard, K. P. Dynamic Mechanical Analysis: A Practical Introduction; CRC Press: Boca Raton, Florida, 1999; p 128.